

Supported Single-Site Organometallic Catalysts for the Synthesis of High-Performance Polyolefins

Madelyn M. Stalzer · Massimiliano Delferro ·
Tobin J. Marks

Received: 3 November 2014 / Accepted: 4 November 2014 / Published online: 18 November 2014
© Springer Science+Business Media New York 2014

Abstract Single-site organometallic catalysts supported on solid inorganic or organic substrates are making an important contribution to heterogeneous catalysis. Early and late transition metal single-site catalysts have changed the polyolefin manufacturing industry and research with their ability to produce polymers with unique properties. Moreover, several of these catalysts have been commercialized on a large scale. Their heterogenization for slurry or gas phase olefin polymerization is important to produce polyolefin as beads and to avoid reactor fouling. The large majority of supports currently used in industry are inorganic materials (SiO_2 , Al_2O_3 , MgCl_2), with silica being the most important. Single-site supported catalysts are most commonly prepared by molecular-level anchoring/chemisorption, in which a molecular precursor undergoes reaction with the surface while maintaining most of the ligand sphere of the parent molecule. Chemisorption of discrete organometallic complexes on solid supports yields catalysts with well-defined active sites, greater thermal stability than the homogeneous analogues, and decreased reactor fouling versus the homogeneous analogues. This review presents a detailed account of the synthesis, characterization and polymerization properties of single-site catalysts supported on metal oxides and metal sulfated oxides, primarily carried out at Northwestern University.

Keywords Heterogeneous catalysis · Homogeneous catalysis · Polymerization

M. M. Stalzer · M. Delferro (✉) · T. J. Marks (✉)
Department of Chemistry, Northwestern University, Evanston,
IL 60208-3113, USA
e-mail: m-delferro@northwestern.edu

T. J. Marks
e-mail: t-marks@northwestern.edu

1 Introduction

Polyolefins are the most widely used class of polymers with a global consumption of approximately 211 million metric tons with an average price on the US market of \$1,422.00 per metric ton [1]. Notwithstanding “green” concerns, polyolefins still surpass biopolymers in performance and energy efficiency [2]. While biopolymers rank high in terms of green design metrics, their production incurs relatively large environmental impact. On the other hand, polyolefins rank first in terms of life cycle assessment. Polyethylene is the simplest (and cheapest) polyolefin, having the general formula $(-\text{CH}_2-)_n$. It is typically a semicrystalline material, with mixture of interconnected crystalline and amorphous regions. In terms of microstructure, different polyethylenes are commercially available, with completely dissimilar chemical, physical, and mechanical properties. Polyethylene is conventionally classified as either: (i) high-density polyethylene (HDPE), (ii) low-density polyethylene (LDPE), or (iii) linear low-density polyethylene (LLDPE). HDPE has small amounts of branching (<1 %), with a density of 0.941 g/cm^3 , LDPE contains a mixture of long (> C_6) and short branches (methyl, ethyl, butyl) with a density of about 0.92 g/cm^3 , while LLDPE has a high content of short branches (< C_6) and a density less than 0.925 g/cm^3 (Fig. 1) [3]. The type and degree of branching underlie many of the differing HDPE, LDPE, and LLDPE physical properties because they affect crystallinity and the extent of amorphous character [4].

Historically, polyolefins were produced using highly active heterogeneous catalysts prepared from supported groups 4 or 6 halides, activated by aluminum alkyls. In the 1950s, the first olefin polymerization catalyst was reported by Phillips Petroleum constituted essentially of Cr/silica or

Fig. 1 Examples of commercial polyethylenes

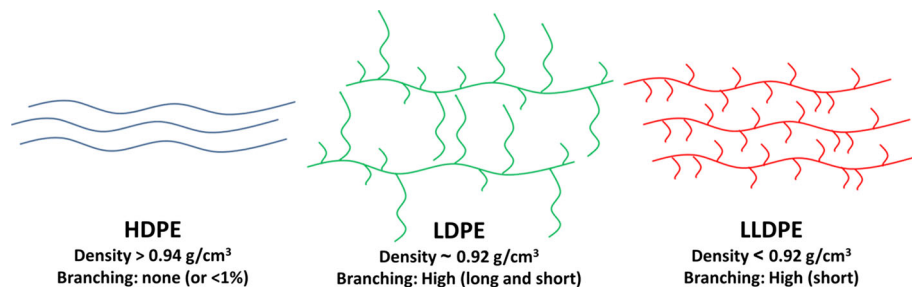


Fig. 2 Proposed structures for Phillips catalyst (left) and supported Ziegler–Natta catalyst on MgCl₂ (right)

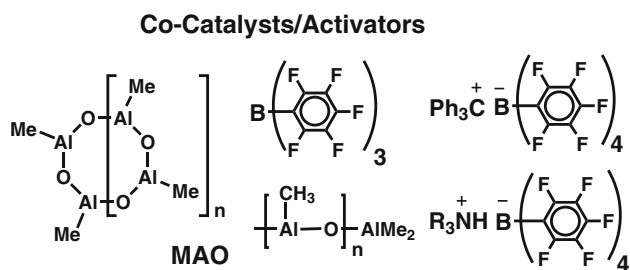
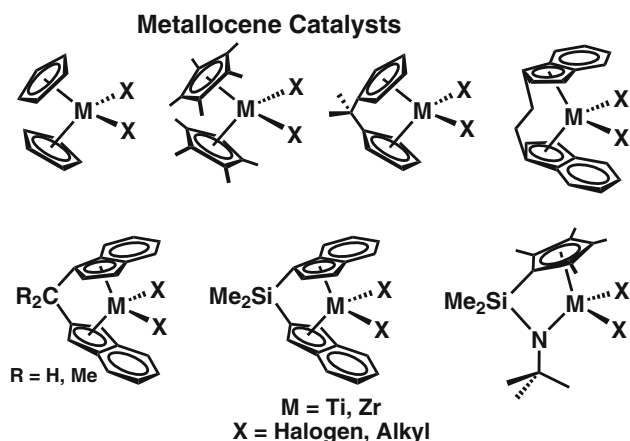
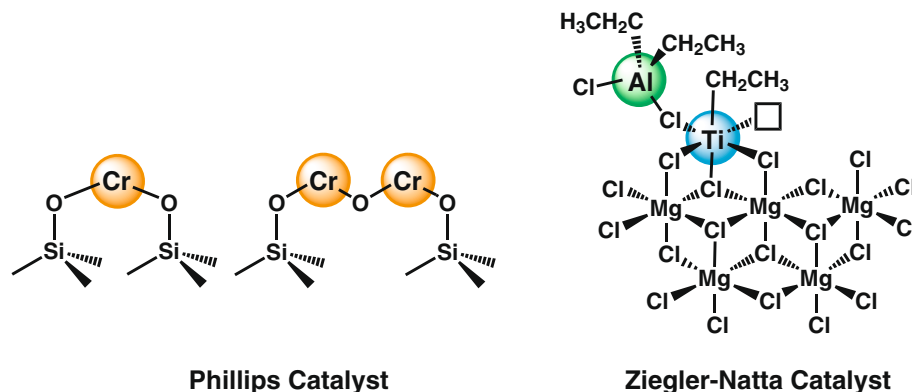


Fig. 3 Selected examples of metallocene precatalysts and activating cocatalysts

Cr/silica–alumina (Fig. 2) [5–7]. This catalyst system, modified and optimized, is used today by various companies around the world, and accounts for a large share

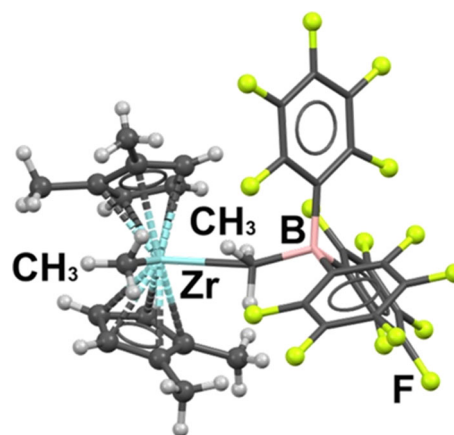


Fig. 4 Molecular structure of the mononuclear ion-pair polymerization catalyst $[(1,2-(\text{CH}_3)_2\text{C}_5\text{H}_3)_2\text{ZrCH}_3]^+[\text{CH}_3\text{B}(\text{C}_6\text{F}_5)_3]^-$. Adapted with permission from J Am Chem Soc (1991) 113:3623–3625 [26]. Copyright 1991 American Chemical Society

(~40 to 50 %) of the world's HDPE production. In 1963 Karl Ziegler and Giulio Natta received the Nobel Prize in Chemistry “for their discoveries in the field of the chemistry and technology of high polymers” [8]. Heterogeneous Ziegler–Natta catalysts are binary combinations of supported TiCl_4 and AlR_3 ($R = \text{alkyl, aryl, hydride}$) on MgCl_2 (Fig. 2), and are still employed on a large scale to produce isotactic polypropylene (*iPP*) and HDPE [9–12]. In the late 1980s, molecule-based group 4 metallocene homogeneous olefin polymerization catalysts emerged from discoveries

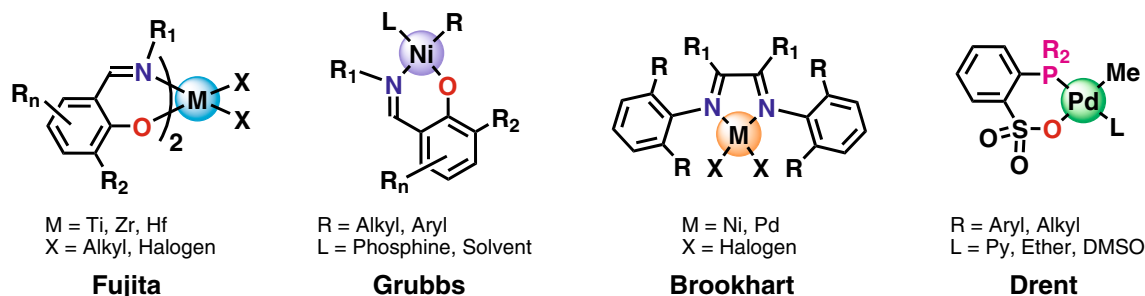


Fig. 5 Examples of non-metallocene olefin polymerization catalysts

by Walter Kaminsky [13–15]. A methylaluminumoxane (MAO, Fig. 3) cocatalyst, a partially hydrolyzed trimethyl aluminium reagent, was found to be an efficient activator for these homogeneous group 4 metallocene catalysts (Fig. 3) [13–15]. This highly active homogeneous system allows for tuning of the product polymer microstructure (M_w , PDI, % comonomer incorporation, tacticity) exclusively by varying the organic ancillary ligands surrounding the group 4 metal [14, 16–24].

Another major advance in olefin polymerization catalysis was the independent discovery in the 1990s by the Marks group [25, 26] at Northwestern and Ewen and co-workers at Exxon Chemical Company [27] of catalytically active, isolable, and structurally well-defined, 1:1 catalyst/cocatalyst ion pairs derived from metallocene dialkyls and the organo-Lewis acid $B(C_6F_5)_3$ (Fig. 4) [28–30].

Detailed thermodynamic/thermochemical and NMR molecular dynamics studies of the ion-paired catalytic systems show that $[L_nM-R]^+[MeB(C_6F_5)_3]^-$ polymerization properties are sensitive to metal ancillary ligation, R substituent, borane acidity, and solvent polarity. These trends can be understood in terms of the ability of the metallocene ancillary ligands to stabilize the cationic charge, the homolytic $M-CH_3$ bond dissociation enthalpies, and the electron withdrawing power of the borane substituents. These new “single-site” catalytic systems are far better defined and more rationally tunable in terms of catalytic activity and product selectivity, structure, thermodynamics, and mechanism, which enable the discovery of new catalysts, cocatalysts, deeper mechanistic understanding of both the homogeneous and heterogeneous systems, and macromolecules with dramatically different properties, and finally, large-scale industrial processes [31].

At the beginning of the 1990s, new generations of “non-metallocene” [32–35] catalysts based on various phenoximinato ligands were reported by Fujita and co-workers (Group 4, Fig. 5) [36–42] and Grubbs and co-workers (Group 10, Fig. 5) [43–46]. In 1995, Brookhart and co-workers reported high activity α -diimine Ni and Pd

complexes which are able to co-polymerize ethylene with polar monomers (Fig. 5) [47–53]. In addition, in early 2000, Drent and co-workers [54] at Shell reported that neutral Pd(II) catalysts generated in situ from phosphonium-sulfonate ligands copolymerize ethylene and methyl acrylate to produce linear copolymers (Fig. 5) [55]. Especially in the case of group 4, these new catalysts and cocatalyst/activators have achieved great success in the production of advanced polyolefin materials [4]. The new systems are able to control product molecular weight, polydispersity, comonomer enchainment level and pattern, the tacticity of poly(α -olefins) [17, 56, 57], copolymerization of olefins with polar comonomers (group 10) [54, 55, 58–62], and the catalytic synthesis of block copolymers by processes such as chain shuttling polymerization [63–67].

Heterogeneous olefin polymerization catalysts offer many distinct attractions, such as thermal robustness, high activity, high degrees of coordinative unsaturation, high product molecular masses, and in some cases, high iso-selectivity. However, understanding structure/reactivity/selectivity relationships in these systems is severely complicated by uncertainties in the active site structure(s) and the percentage(s). For all these reasons, grafting well-defined, single-site homogeneous molecular catalysts on surfaces has emerged as a powerful tool to create new catalysts, to characterize surface species, and thus to establish unambiguous structure/activity relationships [68–73]. For example, it has been shown that well-defined zirconium hydrides supported on alumina are highly active catalysts for alkane hydrogenolysis (Fig. 6a) [74] and silica-supported tungsten [75–78] and molybdenum complexes (Fig. 6b) [79–82] are effective catalysts for alkane metathesis [69, 71, 77, 83–85].

In many cases, the catalytic activities of the supported organometallics far surpass those achievable with the analogous metal complexes in homogeneous system. Also, the structural nature of the molecule-derived adsorbates can be well characterized by a combination of techniques such as solid state NMR, X-ray photoelectron spectroscopy

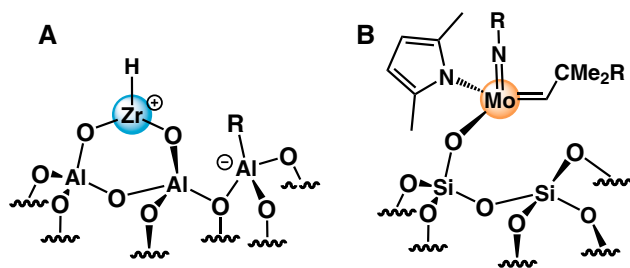


Fig. 6 Selected examples of supported organometallic catalysts

(XPS), vibrational spectroscopy (FT-IR), X-ray absorption spectroscopy (XAS), and density functional theory (DFT) calculations. However despite this progress, many important mechanistic and structural details remain unclear such as (i) the nature of both the catalytically active and catalytically inactive surface species created on chemisorption, including the degree to which the original ligation is preserved; (ii) the number and type of bonds established to the oxide support and the most reactive oxide surface sites for the grafting process; and (iii) the adsorbate structures which maximize catalytic activity. Thus, comparing the key aspects of the adsorbate–oxide surface interaction with the relevant features in well-characterized solution-phase analogues offers an opportunity to better understand the distinctive aspects of the surface organometallic chemistry.

This review focuses primarily on recent research at Northwestern in which organo-groups 4 and 5, and organoactinide complexes are supported on dehydroxylated γ -alumina [86, 87] and sulfated metal oxides [88–90]. The combined application of solid-state NMR spectroscopy, periodic DFT calculations, and metal X-ray absorption spectroscopy indicates formation of organometallic cations having a largely electrostatic $L_n-M^+ \cdots \text{surface}^-$ interaction. It will be also seen that these species are highly active catalysts for α -olefin polymerization and arene hydrogenation, with nearly $\sim 100\%$ of active site in the case of sulfated metal oxide supports.

2 Discussion

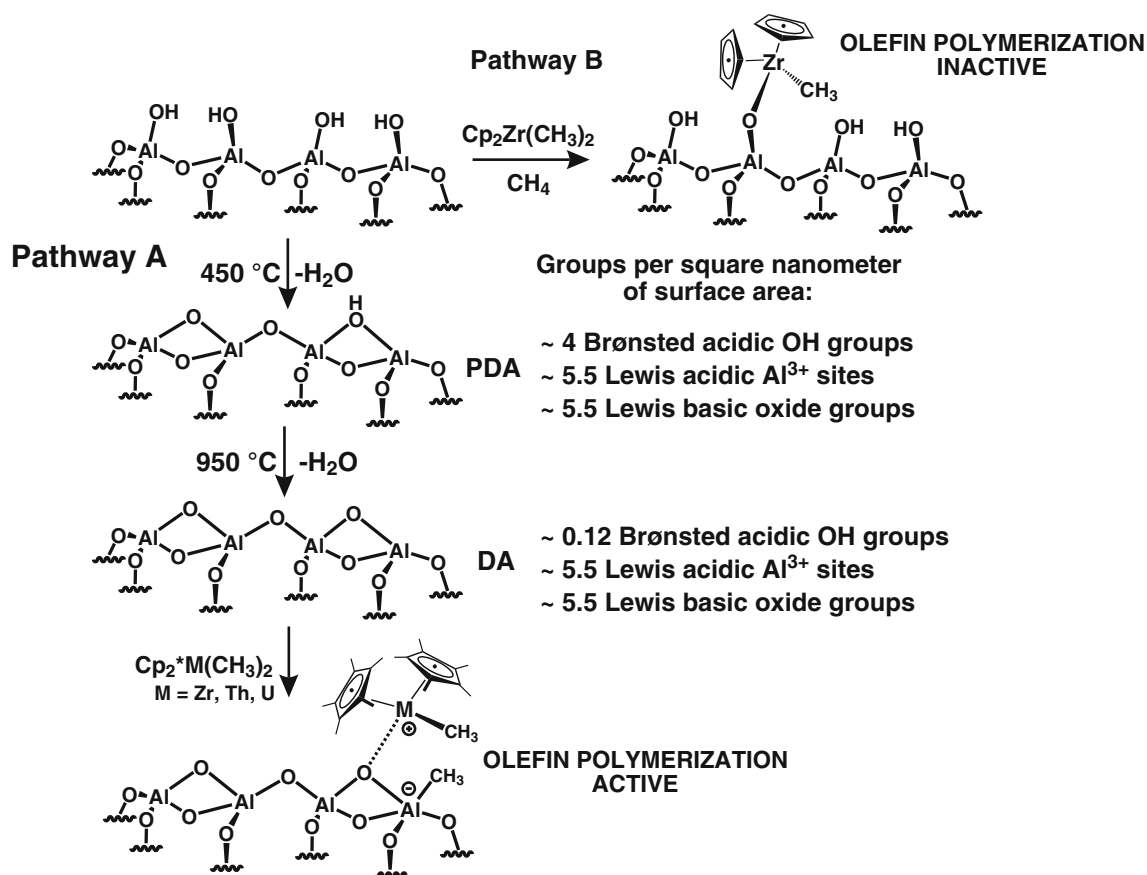
2.1 Dehydroxylated γ -Alumina Supports

Dehydroxylated γ -alumina (DA) and partially dehydroxylated γ -alumina (PDA) surfaces show pronounced Lewis acidic character due to coordinatively unsaturated surface Al sites [74, 91–93] that are reminiscent of analogous MAO cocatalysts and structurally well-defined perfluoroarylborane and borate catalyst activators [28–30]. From a coordination chemistry point of view, the accessibility of both Brønsted and Lewis acid sites on alumina offers a unique complexation environment. DA and PDA substrates

are prepared by heating γ -alumina (Scheme 1) with consequent elimination of water molecules and formation of Al–O–Al moieties [74, 91–93]. Reaction of organometallic precursors with PDA or DA yields highly active catalysts for both olefin and arene hydrogenation and olefin polymerization (vide infra). Heterolytic M–C bond scission is the primary chemisorption mechanism for highly Lewis acidic surfaces [73]. Here the hydrocarbyl anion is transferred to the surface (Lewis acid sites) to give rise to a cationic organometallic adsorbate (Scheme 1, Pathway A). In marked contrast to these results, chemisorption of organometallic precursors on SiO_2 , Al_2O_3 , and SiO_2 – Al_2O_3 surfaces having appreciable coverage by weakly acidic OH groups, predominantly yields covalently bound, poorly electrophilic species via M–CH₃ protonolysis with CH_4 evolution (Scheme 1, Pathway B) [72]. While these sites can be characterized by high-resolution solid state NMR and X-ray adsorption fine structure spectroscopy (EXAFS), they display minimal catalytic turnover in the absence of added activators (e.g., MAO or $\text{B}(\text{C}_6\text{F}_5)_3$), and the fraction of catalytically significant sites is unknown [94, 95].

The ^{13}C CPMAS NMR spectrum of $\text{Cp}_2^*\text{Th}(^{13}\text{CH}_3)_2$ chemisorbed on DA [96] shows the transfer of a methide anion from the actinide center to a quadrupolar Al Lewis acid site on the surface. The Al– $^{13}\text{CH}_3$ resonance appears at the characteristic upfield position ($\delta = -5$ ppm), whereas the downfield shifted Th– $^{13}\text{CH}_3$ signal at $\delta \sim 60$ ppm indicates formation of a “cation-like” electron-deficient organothorium species as in Scheme 1 Pathway A [97–99]. No evidence of Cp^* protonation or redox processes are observed. Interestingly, homogeneous solutions of $\text{Cp}_2^*\text{Th}(\text{CH}_3)_2$ are minimally active for ethylene polymerization and olefin hydrogenation [100–104]. On the other hand, on adsorption DA results in a profound increase in catalytic activity [86, 105]. However, by means of quantitative poisoning experiments using either H_2O or CO as probes, it was shown that only $\sim 4\%$ of the $\text{Cp}_2^*\text{Th}(\text{CH}_3)_2/\text{DA}$ sites are ethylene polymerization/olefin hydrogenation active [86, 96, 104, 106–110].

In order to test the generality of the supported organoactinide chemistry discussed above, group 4 zirconocenes have also been supported on dehydroxylated γ -alumina [111]. Analogous to the ^{13}C CPMAS NMR experiments performed with $\text{Cp}_2^*\text{Th}(^{13}\text{CH}_3)_2$, $\text{Cp}_2\text{Zr}(^{13}\text{CH}_3)_2$ supported on DA produces cationic complexes via methide transfer to the surface, while the same precursor supported on PDA yields both μ -oxo (Scheme 1 Pathway B) and cationic species, indicative of the presence of both weak Brønsted and Lewis acid sites. Measurements of evolved CH_4 during the supporting reaction find similar yields for both thorium and zirconium species on DA, while lower yields were observed for zirconium species on PDA, likely due to the increased protonolytic stability of Zr-alkyl bonds [112].



Scheme 1 Pathway A: synthesis of DA dehydroxylated γ -alumina, PDA partially dehydroxylated γ -alumina, and supported cationic organometallic catalyst. Pathway B: supported neutrally charged μ -oxo organometallic complex on γ -alumina

The catalytic activity of the group 4 complexes was tested for propylene hydrogenation and ethylene polymerization. For those supported on DA, activity was generally found to be approximately 30 % of that of related organoactinide catalysts. However, in marked contrast to organoactinides, organozirconium complexes on PDA also showed reactivity for propylene hydrogenation. Active site measurements for organozirconium complexes on DA indicated that for $\text{Cp}_2\text{Zr}(\text{CH}_3)_2/\text{DA}$, ~4 % of sites are active, and for $\text{Cp}^*\text{Zr}(\text{CH}_3)_3/\text{DA}$, ~12 % are active, roughly mirroring the previous results for organoactinides on DA.

Periodic density functional calculations has been performed to investigate the structural and catalytic properties of the organozirconium precatalyst $\text{Cp}_2\text{Zr}(\text{CH}_3)_2$, chemisorbed on a model dehydroxylated γ -alumina (110) surface [113]. Two different prototypical surface oxide environments, namely μ_3 -O and μ_2 -O, can interact with the $\text{Cp}_2\text{ZrCH}_3^+$ adsorbate (Fig. 7). The interaction of the $\text{Cp}_2\text{ZrCH}_3^+$ adsorbate species with the μ_2 -O sites is far stronger than that with the μ_3 -O sites due to the greater coordinative unsaturation of the former. Moreover, the interaction with the μ_3 -O sites is weaker than that in the

parent homogeneous $\text{Cp}_2\text{ZrCH}_3^+ \text{H}_3\text{CB}(\text{C}_6\text{F}_5)_3^-$ ion pair structure. The energetics of catalytic processes for the chemisorbed $\text{Cp}_2\text{ZrCH}_3^+$ sites for ethylene polymerization was examined at both μ_2 -O and μ_3 -O environments and compared to the analogous homogeneous catalyst. A Cossee enchainment mechanism proceeds via ethylene π -complex formation and an α -agostic assisted transition state to yield γ - and β -agostic insertion products. The overall kinetics of enchainment are closely correlated with the energetics of π -complex formation, and it is suggested that the differing kinetic behaviors of the surface-bound Cp_2ZrR^+ species on the various Al_2O_3 coordination sites and the analogous homogeneous species reflect differences in the olefin π -complex stabilization energies. Specifically, the activation energy for olefin insertion rises in the order μ_3 -O site < homogeneous $\text{Cp}_2\text{ZrCH}_3^+ \text{H}_3\text{CB}(\text{C}_6\text{F}_5)_3^-$ catalyst < μ_2 -O site.

2.2 Sulfated Metal Oxides

Sulfated metal oxides (SMOs) have received significant attention in the past as environmentally friendly

Fig. 7 **a** Dioxo- and **b** oxo-bridged zirconocenium coordination on an alumina μ_2 -O site. **c** Dioxo- and **d** oxo-bridged zirconocenium coordination on a μ_3 -O alumina surface site. Adapted with permission from J Am Chem Soc (2008) 130:16533–16546 [113]. Copyright 2008 American Chemical Society

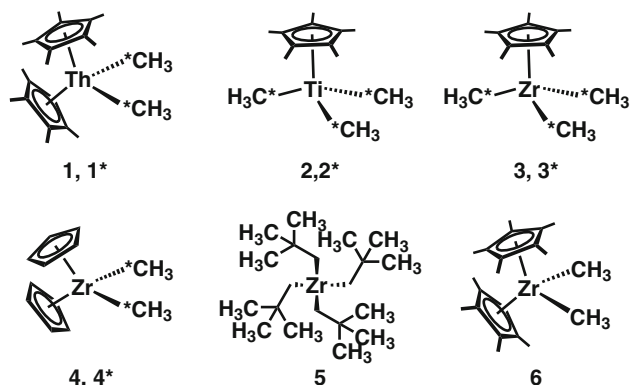
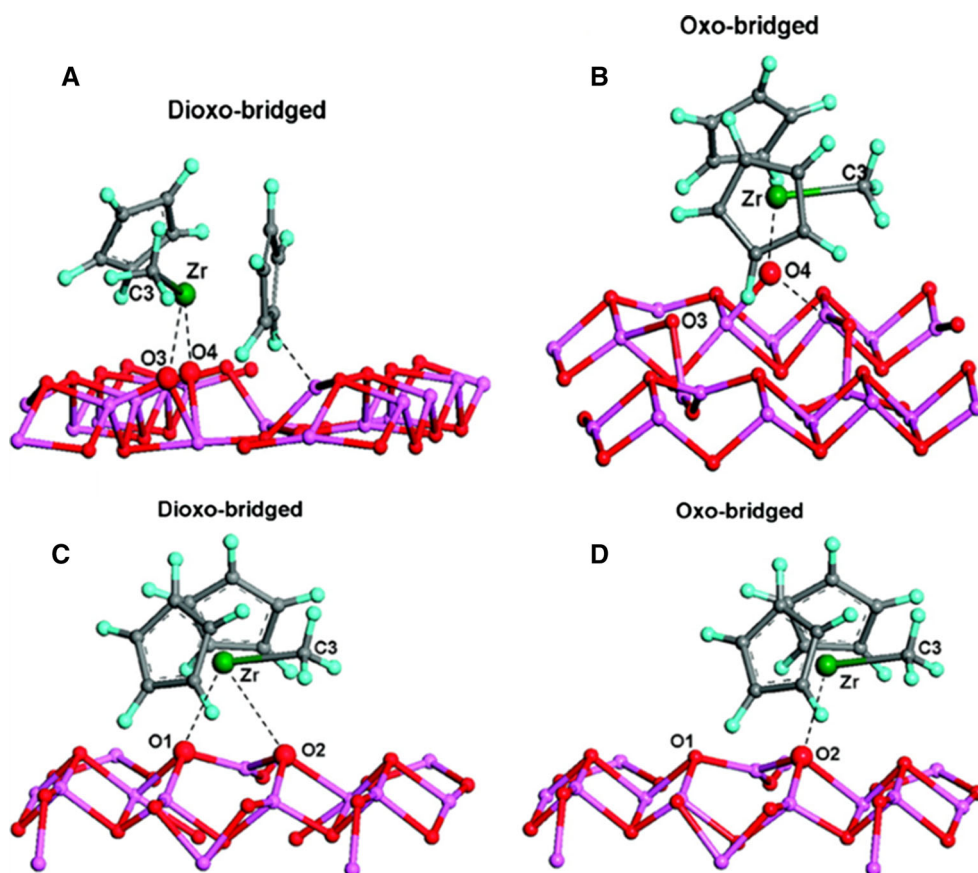


Fig. 8 Molecular precursors for chemisorption on SMOs to produce anchored catalysts

alternatives for superacid catalyzed reactions, such as the skeletal isomerization of alkanes [114] and the production of biodiesel [115]. To this end, a variety of oxides have been sulfated, such as zirconia (ZrS, $H_0 = -16$), alumina (AlS, $H_0 = -14.6$), stannia (SnS, $H_0 = -18$), hematite (FeS, $H_0 = -13$), and titania (TiS, $H_0 = -14.6$), [116] typically by exposure to a sulfation reagent, the most common of which is sulfuric acid, and subsequent calcination. As

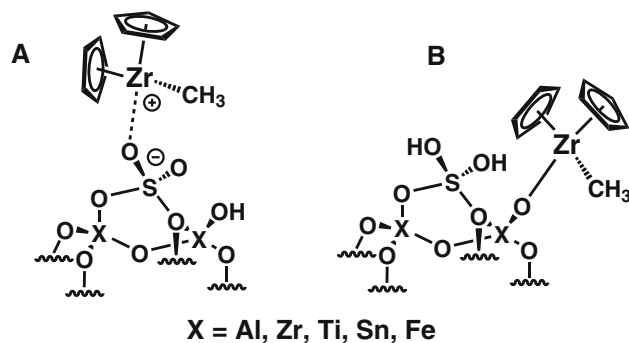
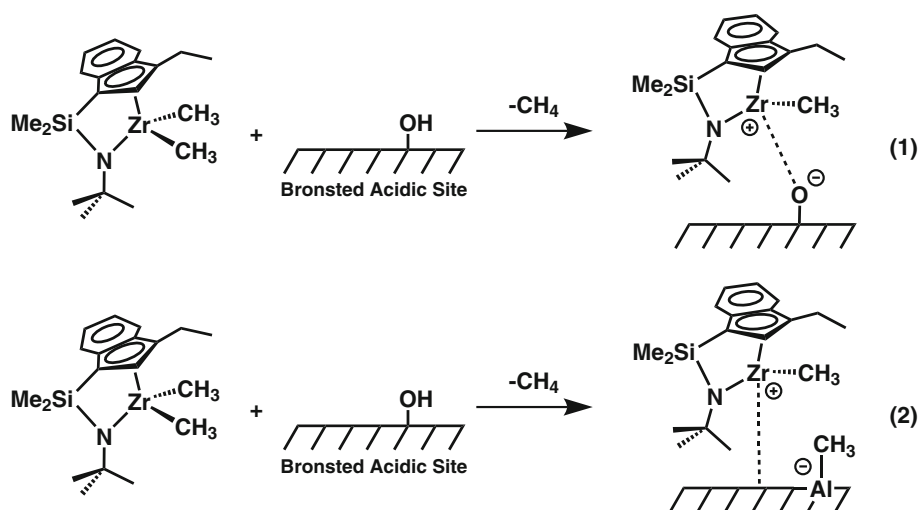


Fig. 9 Proposed structures of zirconocenium complex supported on sulfated metal oxides

supports for single site catalysts, sulfated metal oxides are particularly well-suited due to the presence of a generally large concentration of strong Brønsted and Lewis acid sites, which yield highly active ‘cationic’ metal adsorbate centers (vide supra). Similar to the studies discussed previously with PDA and DA, the use of model adsorbates (Fig. 8) along with ^{13}C CPMAS NMR techniques have been valuable in elucidating the surface character of these SMOs-organometallic complexes/catalysts (Fig. 9).

Scheme 2 Synthesis of monometallic CGC-Zr catalysts supported on sulfated metal oxides



Sulfated zirconia (ZrS) was one of the first SMOs investigated by our group [117–119]. Initial studies of the surface characteristics of ZrS were performed by the chemisorption of ^{13}C labeled $\text{Cp}^*\text{Zr}(\text{CH}_3)_3$ (**1***) [118]. The ^{13}C CPMAS spectrum of **1*/ZrS** compared to that of **1*/DA** revealed important differences in the chemisorption pathways. Specifically, the peak resulting from methide transfer is substantially diminished, suggestive of only a small density of Lewis sites on the ZrS surface. The shift of the $\text{Th-}^{13}\text{CH}_3^+$ resonance to lower field also denotes a more electrophilic ‘cationic’ metal center (Scheme 1, Pathway A), resulting from the greater surface acidity and suggesting a more active catalytic site (vide infra). The minimal presence of hydrocarbyl transfer to the surface and increased electrophilicity of the adsorbate metal center are also confirmed with adsorbates $\text{CpTi}(\text{CH}_3)_2/\text{ZrS}$ (**2*/ZrS**), $\text{Cp}^*\text{Zr}(\text{CH}_3)_2/\text{ZrS}$ (**3*/ZrS**), $\text{Cp}_2\text{Zr}(\text{CH}_3)/\text{ZrS}$ (**4*/ZrS**), and $\text{Zr}(\text{tBu})_3/\text{ZrS}$. **1*/ZrS** is also observed to have the most downfield shifted resonance for $\text{Zr-}^{13}\text{CH}_3^+$ when compared with homogeneous analogues, indicating the highly electrophilic character of the metal center (Scheme 2).

Other SMOs, including AIS [117, 120–123], SnS [117], FeS [117], and TiS [117] were analyzed in a similar way and found to yield analogous surface species. In comparing a given series, it is noted that the magnitude of the shift in resonances between the precursor and the adsorbate qualitatively correlates with the electronic unsaturation of the electrophilic species (Table 1). For **4*** chemisorbed on AIS, SnS, and TiS, mainly ‘cationic’ species (A), with small amounts of μ -oxo (B) present in SnS, are produced via protonolytic chemisorption of **4***, with methide transfer remaining below the detection limits, implying the presence of primarily strong Brønsted sites. For **4*/ZrS**, however, μ -oxo species are formed, with protonolysis by weak Brønsted acid sites dominating, and a small,

Table 1 ^{13}C CPMAS NMR parameters for model adsorbates on various SMOs

Complex	M-CH ₃ (δ)	Cp (δ)
$\text{Cp}_2\text{Zr}(\text{CH}_3)_2$	30.45	110.45
$\text{Cp}_2\text{Zr}^{13}\text{CH}_3/\text{ZrS}$	37.1	114.1
$\text{Cp}_2\text{Zr}^{13}\text{CH}_3/\text{SnS}$	35.7 and 20.5	113.8
$\text{Cp}_2\text{Zr}^{13}\text{CH}_3/\text{FeS}$	37.6 and 21.7	110.7
$\text{Cp}_2\text{Zr}^{13}\text{CH}_3/\text{TiS}$	33.8	113.4
$\text{Cp}^*\text{Zr}^{13}\text{CH}_3$	36.8	117.4
$\text{Cp}^*\text{Zr}^{13}\text{CH}_3/\text{AIS}$	46.0	123.0
$\text{Cp}^*\text{Zr}^{13}\text{CH}_3/n\text{-AIS}$	43.0	123.3

downfield shifted resonance for ‘cationic’ species also observed. Nanoparticles of AIS (n-AIS) [121] yield similar structural results to bulk AIS, except for a larger presence of methide transfer, indicative of a higher density of Lewis acid sites. n-AIS also enables increased loadings of Zr due to minimized internal surface area.

Adsorption of organo-group 4 complexes on AIS was also studied by extended X-ray absorption fine structure (EXAFS) and periodic density function theory (DFT) computation in order to gain a more realistic understanding of the structural characteristics of the adsorbates on SMOs. [120]. Zr K-edge EXAFS data were collected under strictly anhydrous/anaerobic conditions and, due to the structural complexity of the supported moieties, difference spectra (before and after chemisorption) were utilized, since changes in the metal ligation are of primary interest. For **4*/AIS**, the $\text{Zr-O}_{\text{support}}$ bond length is found to be $2.37 \pm 0.02 \text{ \AA}$, which is significantly elongated from typical literature covalent Zr(IV)-OR bond lengths, $2.000 \pm 0.002 \text{ \AA}$ [120], supporting the ^{13}C CPMAS NMR characterization of loose ion pairing between the ‘cationic’ metal adsorbate and the negative charged-delocalized

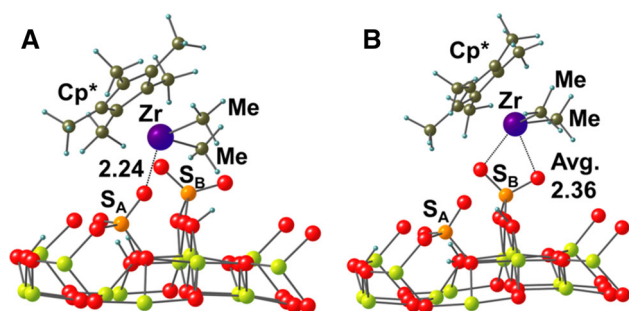


Fig. 10 Energy-minimized computed chemisorbed catalyst structures for: **a** $\text{Cp}^*\text{Zr}(\text{CH}_3)_2^+$ coordination to the $\text{S}=\text{O}$ groups of the sulfated alumina surface at S_A sites. **b** $\text{Cp}^*\text{Zr}(\text{CH}_3)_2^+$ coordination to the $\text{S}=\text{O}$ groups of the sulfated alumina surface at S_B sites. Distances in Å. Avg. = average distance. Zr = purple, C = olive, H = blue, O = red, S = orange, Al = yellow-green. Adapted with permission from Proc Nat Acad Sci USA (2013) 110:413–418 [120]

surface. This is further supported by DFT calculations, which, based on two potential types of sulfate site (Fig. 10), find mean $\text{Zr}-\text{O}_{\text{support}}$ distances of 2.22 and 2.42 Å. As for the interaction between the adsorbate and the surface, the EXAFS difference spectra reveal a $\text{CN} = 2.1$, such that the negative charge on the surface is delocalized between two proximate oxygen atoms that both bind to the metal center. After exposure to benzene under hydrogenation conditions, DFT calculations predict insertion of the benzene between the $\text{Zr}^+\cdots\bar{\text{O}}$ bond, which finds close analogy to the ion pair weakening and anion displacement in activated homogeneous early transition metal polymerization catalysts upon olefin approach/activation.

In the interest of expanding the variety of supported organometallic moieties, constrained geometry catalysts (CGC, Fig. 11) [124] were also chemisorbed onto AIS [122]. CGCs are valued for their increased thermal stability and favorable incorporation of comonomers during polymerization, resulting in long chain branching polymers, due to more open coordination spheres. The formation of cationic surface species was further verified by a distinct color change, from colorless to yellow (for organozirconium complexes) or colorless to orange (for organotitanium complexes), which is analogous to the color change observed during homogenous activation with organo-Lewis acids such as $\text{B}(\text{C}_6\text{F}_5)_3$. For the bimetallic $\mathbf{9}/\text{AIS}$, both the number of metal centers activated (one or both) and the type (protonolytic or methide transfer) of chemisorption permits the exact structural characterization of this adsorbate (Fig. 12). The integration of the $\mathbf{9}/\text{AIS}$ ^{13}C CPMAS NMR resonances suggests that the majority of adsorbate species have both metal centers activated, while the integration of the $\text{Zr}-^{13}\text{C}:\text{Me}:\text{Al}-\text{Me}$ resonances in the ^{13}C CPMAS NMR is found to be 1:0.6, whereas a ratio of $\sim 3:1$ is expected for activation of a single metal

center. Thus, both metals in the bimetallic precursor are likely activated, approximately 40 % by metal-hydrocarbyl protonolytic chemisorption and 60 % by methide transfer to the surface.

Following structural and chemical characterization of the chemisorption pathways, olefin homo- and copolymerizations underscore the catalytic utility of SMOs as activators and weakly coordinating anions. For the catalysts discussed here, the principal product of ethylene polymerization is HDPE with minimal branching and ultrahigh molecular weight, as observed in previous studies of organozirconium hydrocarbyls supported on alumina (vide supra). For ethylene homopolymerizations using ZrS and AIS as supports (118–120; 124), a number of adsorbates with varying electronic and coordinative saturation were assayed (Table 2). In general, polymerization activity is found to increase with increasing coordinative unsaturation, such that $\text{Zr}(\text{CH}_2\text{Ph})_4 > \text{Cp}^*\text{Zr}(\text{CH}_3)_3$ for every SMO. As for support effects, activity follows the trend $\text{ZrS} \geq \text{AIS} > \text{SnS} > \text{FeS} > \text{TiS}$. Importantly, AIS is found to have an ethylene homopolymerization activity almost 10x that of $\text{Cp}^*\text{Zr}(\text{CH}_3)_3/\text{DA}$ (1.2×10^5 g PE/mol Zr h), proving that chemisorption on SMOs yields more active ‘cationic’ centers, reflecting both the increased number of active sites and their ‘cationic’ nature (vide infra). Nanoparticle-AIS is also found to be an effective activator and high surface area support for the rapid production of high molecular weight PE and its performance is found to be solvent dependent, heptane $>$ toluene, likely due to the coordinative inhibition of arenes at the electrophilic active sites [126]. Although solvent dependence was only tested on n-AIS supported catalysts, all SMO adsorbates are expected to exhibit similar behavior due to their mainly ‘cationic’ character.

One of the principal attractions of SMOs is the high percentage of zirconium adsorbate sites that are catalytically significant. In situ kinetic poisoning experiments performed on the above catalysts reveal the high number of active sites, with >60 % for all SMOs except FeS attainable, compared to ~ 12 % for $\text{Cp}^*\text{Zr}(\text{CH}_3)_3/\text{DA}$ and <6 % for $\text{Zr}(\text{CH}_2\text{CMe}_2\text{Ph})_4/\text{PDA}$ [112]. While there is no direct correlation between acidity and percentage active sites, for the SMOs discussed here, it appears that materials with $\text{H}_0 < -14$ have a high percentage of active sites. It has been concluded that the exceptional catalytic activity of these zirconium hydrocarbyl adsorbate catalysts reflects an interplay of both the high percentage of active sites and the electrophilicity of such sites, such that both are required for an active catalyst. For example, TiS as a support has 63 ± 9 % active sites, but ^{13}C CPMAS NMR reveals that most of these are of the active μ -oxo type (vide supra), thus the catalyst performs relatively poorly. The attraction of using SMOs as supports/activators thus lies in the fact that

Fig. 11 Mononuclear and binuclear CGC-zirconium catalysts

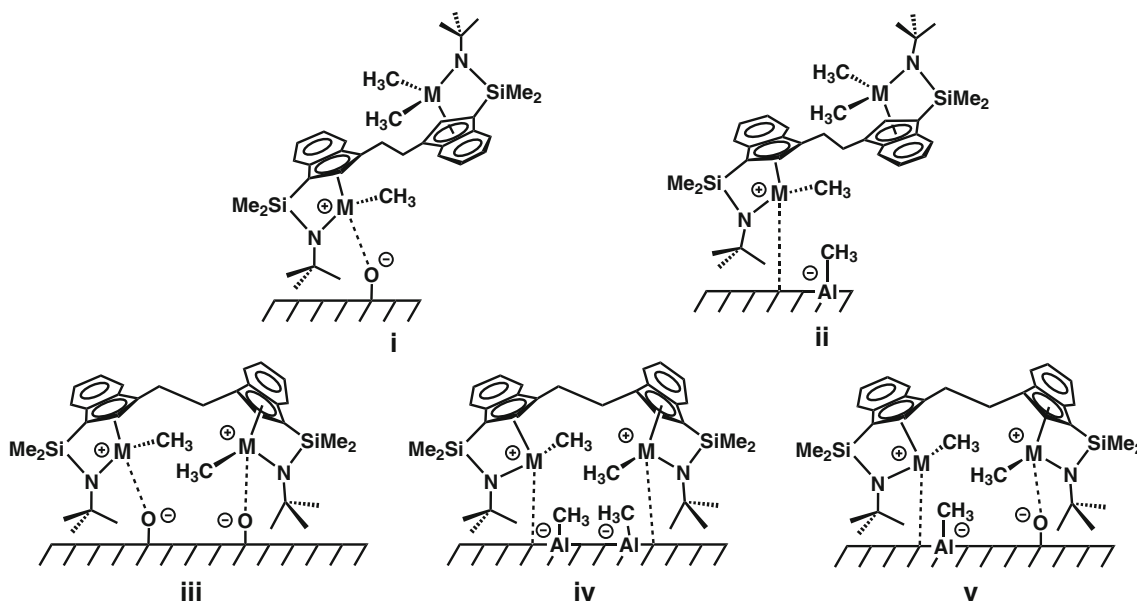
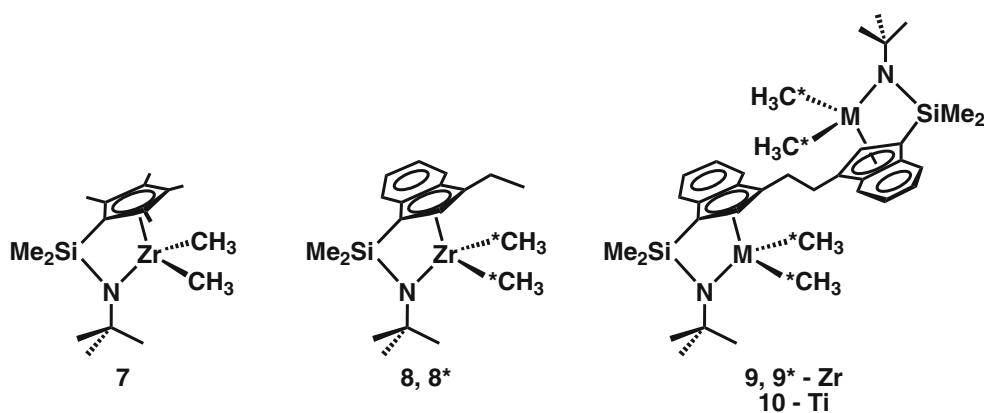


Fig. 12 Potential binding modes of 9/AIS or 10/AIS. As determined by the type and concentration of acid sites: (i) Single metal center protonolytically chemisorbed on a strong Brønsted acid site; (ii) Single metal center chemisorbed via methide transfer on a Lewis acid site; (iii) Both metal centers protonolytically chemisorbed on proximate

strong Brønsted centers; (iv) Both metal centers chemisorbed via methide transfer on proximate Lewis acid sites; (v) One metal center protonolytically chemisorbed, the other chemisorbed by methide transfer

they provide both highly active electrophilic single catalytic sites, and due to their high acidity, nearly 100 % of these sites are catalytically active.

The CGC catalysts supported on AIS were also evaluated for ethylene homopolymerization, along with ethylene/1-hexene copolymerization [122]. Ethylene homopolymerizations are found to yield high molecular weight PE as determined by DSC, and to be highly crystalline with low branch densities, but in all cases, the corresponding supported catalysts have lower catalytic activity than the homogenous analogs, which is attributed to steric repulsion of the support and the adsorbate ligands. Analogously to homogeneous systems [127], the bimetallic Ti_2/AIS is more active than bimetallic Zr_2/AIS . Concerning ethylene/1-hexene copolymerizations,

the supported catalysts are again less active than their homogenous equivalents. Minimal comonomer enchainment is observed (T_m depressed only 3–5 °C from the homopolymer) and it is likely that the steric bulk of the bimetallic Zr_2 and Ti_2 limits 1-hexene approach, thereby frustrating the bimetallic cooperativity observed in homogenous systems.

3 Conclusion and Prospectus

This Review analyzes the effects on olefin polymerization by single-site catalysts supporting them on various oxides and sulfated oxides. The well-established synthetic routes to achieve single-site heterogeneous catalysts and the diverse

Table 2 Ethylene homopolymerization data for SMO supported zirconium hydrocarbyls

Entry	Support	Zr hydrocarbyl	Activity ^c × 10 ⁵	T _m (°C)	Active sites ^d %	Acidity ^e H ₀
1	ZrS	Cp*Zr(CH ₃) ₃	7.7	133.1	~65 ^f	-16
2	ZrS	Zr(CH ₂ Ph) ₄	25	134.0		
3	AlS	Cp*Zr(CH ₃) ₃	11	133.6	87 ± 3	-14.6
4	AlS	Zr(CH ₂ Ph) ₄	21	134.2		
5	SnS	Cp*Zr(CH ₃) ₃	0.98	136.1	61 ± 5	-18
6	SnS	Zr(CH ₂ Ph) ₄	6.6	135.1		
7	FeS	Cp*Zr(CH ₃) ₃	0.24	134.2	22 ± 2	-13 ^g
8	FeS	Zr(CH ₂ Ph) ₄	5.1	135.2		
9	TiS	Cp*Zr(CH ₃) ₃	0.012	138.4	63 ± 9	-14.6
10	TiS	Zr(CH ₂ Ph) ₄	0.63	138.0		

^a Carried out at 60 °C, 150 psi of ethylene, 5.0 mL toluene

^b Cp* = η⁵-C₅Me₅

^c Units: grams of total polymer/(mol Zr h)

^d Number of active sites determined by poisoning ethylene polymerization of Cp*Zr(CH₃)₃/SMO with neopentyl alcohol

^e From Ref [89], measured by the spectrophotometric indicator method, except for SnS from Ref. [125]

^f From Ref [118] Number of active sites determined by poisoning benzene hydrogenation of Cp*Zr(CH₃)₃/ZrS with H₂O

^g Estimated from TDP and activity for butane isomerization due to competing optical properties of the support

techniques (SS NMR, EXAFS, DFT calculations) for their characterization are described. Solid state NMR and EXAFS studies show that alkyl migration from the organometallic precursor to the Lewis acidic sites constitutes the principal adsorption pathway on dehydroxylated alumina (DA), whereas the chemisorption of the same organometallic molecules on highly Brønsted “super-acidic” sulfated metal oxides yields, via Zr-CH₃ protonolysis with methane evolution, highly electrophilic adsorbate species. The resulting “cation-like” species, reminiscent of the homogeneous analogues, are highly active heterogeneous catalysts for olefin polymerization and hydrogenation, with generally high percentages of catalytically significant sites. In many cases, extraordinarily high percentages (~100 %) of catalytically significant sites can be attained, permitting accurate structure determination and isolation/characterization of reaction intermediates.

Acknowledgments Financial support by DOE Basic Energy Sciences (Grant 86ER13511) is gratefully acknowledged.

References

- ACS Division of Polymer Chemistry: Advances in Polyolefins 2013, Santa Rosa
- Tabone MD, Cregg JJ, Beckman EJ, Landis AE (2010) *Environ Sci Technol* 44:8264–8269
- James DE (1985) In: Mark HF, Bikales NM, Overberger CG, Menges G (eds) *Linear low density polyethylene in encyclopedia of polymer science and engineering*, vol 6. Wiley-Interscience, New York, pp 429–454
- Munstedt H (2011) *Soft Matter* 7:2273–2283
- Theopold KH (2014) *Proc Natl Acad Sci USA* 111:11578–11579
- McDaniel MP (2010) *Adv Catal* 53:123–606
- Zecchina A, Groppo E, Damin A, Prestipino C (2005) *Top Organomet Chem* 16:1–35
- http://nobelprize.org/nobel_prizes/chemistry/laureates/1963/
- Abedi S, Abdouss M (2014) *Appl Catal A* 475:386–409
- Claverie JP, Schaper F (2013) *MRS Bull* 38:213–218
- Eisch JJ (2012) *Organometallics* 31:4917–4932
- Corradini P, Guerra G, Cavallo L (2004) *Acc Chem Res* 37:231–241
- Kaminsky W (2012) *Macromolecules* 45:3289–3297
- Kaminsky W, Funck A, Haehnsen H (2009) *Dalton Trans* 41:8803–8810
- Kaminsky W (2004) *J Polym Sci A* 42:3911–3921
- Wang B (2006) *Coord Chem Rev* 250:242–258
- Razavi A, Thewalt U (2006) *Coord Chem Rev* 250:155–169
- Mohring PC, Coville NJ (2006) *Coord Chem Rev* 250:18–35
- Wang W, Wang L (2003) *J Polym Mater* 20:1–8
- Kulshreshtha AK, Awasthi SK (2000) *Pop Plast Packag* 45:53–57
- Kristen MO (1999) *Top Catal* 7:89–95
- Chien JCW (1999) *Top Catal* 7:23–36
- Ban HT, Arai T, Ahn C-H, Uozumi T, Soga K (1999) *Curr Trends Polym Sci* 4:47–64
- Ciardelli F, Altomare A, Michelotti M (1998) *Catal Today* 41:149–157
- Yang X, Stern CL, Marks TJ (1994) *J Am Chem Soc* 116:10015–10031
- Yang X, Stern CL, Marks TJ (1991) *J Am Chem Soc* 113:3623–3625
- Ewen JA, Elder MJ (1996) *Eur Patent Appl* 0,427,697, 1991; US Patent 5,561,092, 1996
- Bochmann M (2010) *Acc Chem Res* 43:1267–1278
- Bochmann M (2010) *Organometallics* 29:4711–4740
- Chen EYX, Marks TJ (2000) *Chem Rev* 100:1391–1434
- Chum PS, Swogger KW (2008) *Progress Poly Sci* 33:797–819

32. Delferro M, Marks TJ (2011) *Chem Rev* 111:2450–2485
33. Budagumpi S, Kim K-H, Kim I (2011) *Coord. Chem Rev* 255:2785–2809
34. Gibson VC, Spitzmesser SK (2003) *Chem Rev* 103:283–315
35. Trifonov AA (2007) *Russ Chem Rev* 76:1051–1072
36. Fujita T, Kawai K (2014) *Top Catal* 57:852–877
37. Iwashita A, Chan MCW, Makio H, Fujita T (2014) *Catal Sci Technol* 4:599–610
38. Kawai K, Fujita T (2009) *Top Organomet Chem* 26:3–46
39. Makio H, Fujita T (2009) *Acc Chem Res* 42:1532–1544
40. Makio H, Terao H, Iwashita A, Fujita T (2011) *Chem Rev* 111:2363–2449
41. Matsugi T, Fujita T (2008) *Chem Soc Rev* 37:1264–1277
42. Mitani M, Saito J, Ishii S-I, Nakayama Y, Makio H et al (2004) *Chem Rec* 4:137–158
43. Connor EF, Younkin TR, Henderson JI, Waltman AW, Grubbs RH (2003) *Chem Commun* 18:2272–2273
44. Connor EF, Younkin TR, Henderson JI, Hwang S, Grubbs RH et al (2002) *J Polym Sci A* 40:2842–2854
45. Younkin TR, Connor EF, Henderson JI, Friedrich SK, Grubbs RH, Bansleben DA (2000) *Science* 287:460–462
46. Wang C, Friedrich S, Younkin TR, Li RT, Grubbs RH et al (1998) *Organometallics* 17:3149–3151
47. Tempel DJ, Johnson LK, Huff RL, White PS, Brookhart M (2000) *J Am Chem Soc* 122:6686–6700
48. Ittel SD, Johnson LK, Brookhart M (2000) *Chem Rev* 100:1169–1203
49. Svejda SA, Johnson LK, Brookhart M (1999) *J Am Chem Soc* 121:10634–10635
50. Mecking S, Johnson LK, Wang L, Brookhart M (1998) *J Am Chem Soc* 120:888–899
51. Rix FC, Brookhart M, White PS (1996) *J Am Chem Soc* 118:4746–4764
52. Johnson LK, Mecking S, Brookhart M (1996) *J Am Chem Soc* 118:267–268
53. Johnson LK, Killian CM, Brookhart M (1995) *J Am Chem Soc* 117:6414–6415
54. Drent E, van Dijk R, van Ginkel R, van Oort B, Pugh RI (2002) *Chem Commun* 1:744–745
55. Nakamura A, Anselment TMJ, Claverie J, Goodall B, Jordan RF et al (2013) *Acc Chem Res* 46:1438–1449
56. Wang X, Wang Y, Shi X, Liu J, Chen C, Li Y (2014) *Macromolecules* 47:552–559
57. Miyake GM, Chen EYX (2011) *Polym Chem* 2:2462–2480
58. Ito S, Nozaki K (2010) *Chem Rec* 10:315–325
59. Goodall BL (2009) *Top Organomet Chem* 26:159–178
60. Popeney CS, Camacho DH, Guan Z (2007) *J Am Chem Soc* 129:10062–10063
61. Soula R, Saillard B, Spitz R, Claverie J, Llauro MF, Monnet C (2002) *Macromolecules* 35:1513–1523
62. Meneghetti SP, Kress J, Lutz PJ (2000) *Macromol Chem Phys* 201:1823–1832
63. Valente A, Stoclet G, Bonnet F, Mortreux A, Visseaux M, Zinck P (2014) *Angew Chem Int Ed* 53:4638–4641
64. Mohammadi Y, Ahmadi M, Saeb MR, Khorasani MM, Yang P, Stadler FJ (2014) *Macromolecules* 47:4778–4789
65. Wenzel TT, Arriola DJ, Carnahan EM, Hustad PD, Kuhlman RL (2009) *Top Organomet Chem* 26:65–104
66. Kuhlman RL, Wenzel TT (2008) *Macromolecules* 41:4090–4094
67. Arriola DJ, Carnahan EM, Hustad PD, Kuhlman RL, Wenzel TT (2006) *Science* 312:714–719
68. Wegener SL, Marks TJ, Stair PC (2012) *Acc Chem Res* 45:206–214
69. Basset J-M, Coperet C, Soulivong D, Taoufik M, Thivolle Cazat J (2010) *J Acc Chem Res* 43:323–334
70. Thomas A, Driess M (2009) *Angew Chem Int Ed* 48:1890–1892
71. Basset J-M, Coperet C, Soulivong D, Taoufik M, Thivolle-Cazat J (2006) *Angew Chem Int Ed* 45:6082–6085
72. Coperet C, Chabanas M, Saint-Arroman RP, Basset J-M (2003) *Angew Chem Int Ed* 42:156–181
73. Marks TJ (1992) *Acc Chem Res* 25:57–65
74. Joubert J, Delbecq F, Thieuleux C, Taoufik M, Blanc F et al (2007) *Organometallics* 26:3329–3335
75. Conley MP, Mougél V, Peryshkov DV, Forrest WP, Gajan D et al (2013) *J Am Chem Soc* 135:19068–19070
76. Merle N, Girard G, Popoff N, De Mallmann A, Bouhoute Y et al (2013) *Inorg Chem* 52:10119–10130
77. Popoff N, Mazoyer E, Pelletier J, Gauvin RM, Taoufik M (2013) *Chem Soc Rev* 42:9035–9054
78. Rhers B, Salameh A, Baudouin A, Quadrelli EA, Taoufik M et al (2006) *Organometallics* 25:3554–3557
79. Blanc F, Thivolle-Cazat J, Basset J-M, Coperet C, Hock AS et al (2007) *J Am Chem Soc* 129:1044–1045
80. Blanc F, Basset J-M, Coperet C, Sinha A, Tonzetich ZJ et al (2008) *J Am Chem Soc* 130:5886–5900
81. Blanc F, Berthoud R, Coperet C, Lesage A, Emsley L et al (2008) *Proc Natl Acad Sci USA* 105:12123–12127
82. Blanc F, Rendon N, Berthoud R, Basset JM, Coperet C, et al (2008) *Dalton Trans* 3156–3158. doi:10.1039/b805686m
83. Buchmeiser MR (2009) *Chem Rev* 109:303–321
84. Deraedt C, d'Halluin M, Astruc D (2013) *Eur J Inorg Chem* 2013:4881–4908
85. Thieuleux C, Coperet C, Dufaud V, Marangelli C, Kuntz E, Basset JM (2004) *J Mol Catal A* 213:47–57
86. Eisen MS, Marks TJ (1994) *J Mol Catal* 86:23–50
87. Rascon F, Wischert R, Coperet C (2011) *Chem Sci* 2:1449–1456
88. Arata K (2009) *Green Chem* 11:1719–1728
89. Arata K (1996) *Appl Catal A* 146:3–32
90. Arata K (1991) *Trends Phys Chem* 2:1–24
91. Delgado M, Delbecq F, Santini CC, Lefebvre F, Norsic S et al (2012) *J Phys Chem C* 116:834–843
92. Wischert R, Florian P, Coperet C, Massiot D, Sautet P (2014) *J Phys Chem C* 118:15292–15299
93. Wischert R, Laurent P, Coperet C, Delbecq F, Sautet P (2012) *J Am Chem Soc* 134:14430–14449
94. Popoff N, Gauvin RM, De Mallmann A, Taoufik M (2012) *Organometallics* 31:4763–4768
95. Millot N, Soignier S, Santini CC, Baudouin A, Basset JM (2006) *J Am Chem Soc* 128:9361–9370
96. Toscano PJ, Marks TJ (1985) *J Am Chem Soc* 107:653–659
97. Chen Y-X, Stern CL, Yang S, Marks TJ (1996) *J Am Chem Soc* 118:12451–12452
98. Yang X, Stern C, Marks TJ (1991) *Organometallics* 10:840–842
99. Lin Z, Le Marechal JF, Sabat M, Marks TJ (1987) *J Am Chem Soc* 109:4127–4129
100. Fendrick CM, Schertz LD, Day VW, Marks TJ (1988) *Organometallics* 7:1828–1838
101. Fagan PJ, Manriquez JM, Vollmer SH, Day CS, Day VW, Marks TJ (1981) *J Am Chem Soc* 103:2206–2220
102. Fagan PJ, Moloy KG, Marks TJ (1981) *J Am Chem Soc* 103:6959–6962
103. Fagan PJ, Manriquez JM, Maatta EA, Seyam AM, Marks TJ (1981) *J Am Chem Soc* 103:6650–6667
104. Bowman RG, Nakamura R, Fagan PJ, Burwell RL Jr, Marks TJ (1981) *J Chem Soc Chem Commun* 6:257–258
105. Eisen MS, Marks TJ (1992) *J Am Chem Soc* 114:10358–10368
106. Eisen MS, Marks TJ (1992) *Organometallics* 11:3939–3941
107. Gillespie RD, Burwell RL Jr, Marks TJ (1991) *Catal Lett* 9:363–368
108. Finch WC, Gillespie RD, Hedden D, Marks TJ (1990) *J Am Chem Soc* 112:6221–6232

109. Toscano PJ, Marks TJ (1986) *Langmuir* 2:820–823
110. He MY, Xiong G, Toscano PJ, Burwell RL Jr, Marks TJ (1985) *J Am Chem Soc* 107:641–652
111. Dahmen KH, Hedden D, Burwell RL, Marks TJ (1988) *Langmuir* 4:1212–1214
112. Schock LE, Marks TJ (1988) *J Am Chem Soc* 110:7701–7715
113. Motta A, Fragala IL, Marks TJ (2008) *J Am Chem Soc* 130:16533–16546
114. Hino M, Kobayashi S, Arata K (1979) *J Am Chem Soc* 101:6439–6441
115. Su F, Guo Y (2014) *Green Chem* 16:2934–2957
116. Corma A (1995) *Chem Rev* 95:559–614
117. Nicholas CP, Marks TJ (2004) *Langmuir* 20:9456–9462
118. Ahn H, Nicholas CP, Marks TJ (2002) *Organometallics* 21:1788–1806
119. Ahn H, Marks TJ (1998) *J Am Chem Soc* 120:13533–13534
120. Williams LA, Guo N, Motta A, Delferro M, Fragala IL et al (2013) *Proc Natl Acad Sci USA* 110:413–418
121. Williams LA, Marks TJ (2011) *ACS Catal* 1:238–245
122. Williams LA, Marks TJ (2009) *Organometallics* 28:2053–2061
123. Nicholas CP, Ahn H, Marks TJ (2003) *J Am Chem Soc* 125:4325–4331
124. Braunschweig H, Breitling FM (2006) *Coord Chem Rev* 250:2691–2720
125. Matsuhashi H, Miyazaki H, Kawamura Y, Nakamura H, Arata K (2001) *Chem Mater* 13:3038–3042
126. Stalzer MM, Gu W, Nicholas CP, Bhattacharyya A, Motta A, Gallagher JR, Zhang G, Miller JT, Delferro M, Marks TJ (unpublished results)
127. McInnis JP, Delferro M, Marks TJ (2014) *Acc Chem Res* 47:2545–2557